Development and experimental validation of a simulation model for open joint ventilated facades

Cristina Sanjuan[a], María José Suárez [b], Eduardo Blanco [b], M.R. Heras [a]

[a]*Department of Energy, Energy Efficiency in Buildings Unit, CIEMAT, 28040 Madrid, Spain*

[b]*Universidad de Oviedo, EDZE (Energía), Campus de Viesques, 33271 Gijón, Asturias, Spain*

Abstract

The investigation of the thermal and fluid dynamical behaviour of Open Joint Ventilated Facades is a challenging task due to the complex airflows generated inside of the naturally ventilated cavity by the existence of open joints. For this reason, the use of advanced fluid measurement and simulation techniques is highly recommended. This paper focuses in the development and experimental validation of a simulation model for these façade systems. More specifically, different turbulence and radiation models available in the commercial computational fluid dynamic codes have been tested on a three-dimensional model and the results have been compared to particle image velocimetry measurements. The correlation between experimental and numerical data has been used in order to select the simulation procedure for this type of facades. Best fittings have been found when using the RNG k-epsilon turbulence model and the Discrete Ordinate radiation model. Using the selected scheme, parametrical simulations have been performed to investigate the effect of increasing the cavity height, and correspondingly, the number of slabs. Results show that ventilation air flow inside the cavity is enhanced by incident radiation as well as by the height of the façade.

Keywords: ventilated facades, CFD validation, turbulence models, and PIV techniques.

1. Introduction

Generalising about the fluid and thermal performance of open joint ventilated facades (OJVF) is somehow difficult because of the big range of constructive solutions existing in the market. Slabs can be metallic, ceramic or made from stone. Additionally, the dimensions and proportions of the slabs, the shape and size of the open joints, as well as the metallic structure frame supporting the exterior coating differ from manufacturer to manufacturer. Apart from the difficulties derived from the constructive solutions, the existence of open joints distributed along the exterior coating has a great influence in the fluid and thermal behaviour of this façade system in comparison to other continuous ventilated facades, such as double glazed ventilated facades (DGVF), whose behaviour is rather well known, as detailed in the studies made by Manz [1], Safer et al. [2], Baldinelli [3], Fuliotto et al. [4] and Coussirat et al. [5] among other authors. The existence of open joints enables the outdoor air to freely enter and leave the ventilated cavity all along the wall, producing discontinuities and instabilities in the flow inside the ventilated cavity, which is highly dependent not only in the façade geometry by also on the solar incident radiation, outdoor temperature and wind conditions. All these factors, summed to the general lack of data related to these construction systems and the absence of validated models, evidence that there is still a lot of work to do before having a global criterion to determine the energy behaviour of OJVF.

In fact, most technical studies concerning open joint ventilated facades have confined themselves to construction solutions and examining the properties of the materials used in them. The current building standards consider this façades, by default, as ordinary ventilated or slightly ventilated air chamber façades without taking into account their fluid behaviour (CTE [6]). Moreover, the commercial building energy simulation software such as VisualDOE [7], TRNSYS [8] or Energy Plus [9] have not yet included a general purpose model to simulate these façade systems. As a consequence, its actual fluid dynamic behaviour and its performance in terms of energy saving and comfort conditions is not yet sufficiently known. For these reasons, an extensive research of the thermal and fluid behaviour of open joint ventilated facades is thus required in order to turn into reality the claimed advantages (their ability to reduce cooling thermal loads) of these construction systems.

In the last years, some studies related to bottom and top ventilated façades with an opaque outer layer have been published. For example, Griffith [10] proposed a model that was later adopted by the Energy Plus simulation package [9]. It is also significant the

computational fluid dynamic (CFD) modelling of a 2D ventilated ceramic façade carried out by Mesado et al. [11], and the work of Patania et al. [12] which is a study of the fluid and thermal energy performance of three façade types under different temperature and radiation conditions, reporting energy saving rates for the summer period. However, all these models do not consider open joints between the slabs. In their previous works, Sanjuan et al [13] and Gonzalez et al. [14, 15], investigated the thermal and fluid dynamic phenomena taking place in open joint ventilated facades under solar radiation. They simulated a 2.4 m high ventilated façade composed of four slabs and the corresponding five joints, and compared it to a conventional façade with sealed cavity. Temperatures, velocity profiles and heat fluxes transferred to the room were analysed and discussed. The authors concluded that temperatures in OJVF under radiation conditions are lower than temperatures in the conventional façades with sealed cavity, which means less heat is transferred to the room. The authors also provided a methodology to quantify the energy savings produced by OJVF and compared the results with simplified models of a ventilated cavity used in energy simulation software of buildings. Following the same methodology, Millar et al. [16] simulated also a 2.4 m high ventilated façade composed of nine slabs and ten horizontal joints, and compared its thermal and fluid behaviour to a top and bottom ventilated façade with opaque outer layer. They have obtained significant conclusions although these models have not been validated.

During 2010, Marinosci et al. [17] investigated experimentally and numerically the thermal behaviour of a real ventilated façade. The authors performed temperature, radiation, and velocity measurements in a ventilated façade of a test building with a squared base of 2.89m and a total height of 7.75 m. The modelling of the façade was made using the software ESP-r and three different air flow nodal network models were tested. The differences of the models depended on whether the joints along the façade were considered sealed or opened. Good agreement between experimental and numerical data was shown when considering the open joints in the modelling. However, very little information on the fluid behaviour of the air inside the ventilated cavity can be extracted from this work.

Also recently, Sanjuan et al. [18] investigated experimentally the fluid and thermal behaviour of an OJVF model in conditions of calm weather and solar radiation. The experimental set up was composed of four slabs and five horizontal joints with a reduced height of 0.825 m. Velocity and temperature measurements were carried out for different heating (solar radiation) conditions. The velocity vector fields were measured with a particle image velocimetry (PIV) system at the vertical centerplane of the cavity. The temperatures in the centre of the slabs and inside the air cavity were measured with Pt100 probes. Additionally, infrared imaging of the slabs surface was also performed. The main features of the flow inside the ventilated cavity are described in the cited reference. The resulting vector fields showed good agreement with previous numerical studies and, in general terms it was observed that the heating of the slabs produces an ascending, but inhomogeneous ventilation flow inside the cavity, that enters though the lower joints and leaves though the upper joints.

The description of the heat and mass transfer phenomena given in the previous works confirms the fact that the complexity of the fluid flow in the regions near the joints and along the ventilated cavity defies analytical methods, making compulsory the use of advanced fluid dynamic simulation techniques, at least in the first stages of the investigation, until all the phenomena taking place are sufficiently known. Nevertheless, the main limitation of the previous cited works relies in the fact that the analysis was performed over specific geometries, making it impossible to expand the results and give a general criterion on the performance of OJVF. Moreover, the application of advanced experimental techniques such as PIV is very laborious, expensive, and restricted to controlled laboratory experiments. For this reason it is very important that numerical models are validated in order to extend its applicability. Once validated, a simulation model can be used in a big range of OJVF geometries and outdoor conditions without the necessity of performing costly experimental measurements.

In a CFD simulation there are some factors that can be intrinsically tested, as the grid, differencing scheme or convergence. Other mathematical tools are more difficult to check or they even depend on the test characteristics. In the OJVF case, these are mainly the procedures employed to simulate the turbulence and radiation. The objective of this work is thus to investigate the suitability of the different turbulence and radiation models available in the commercial CFD codes, to simulate the fluid and thermal performance of OJVF under radiation conditions. The numerical results are compared to PIV measurements performed by Sanjuan et al. [18]. To allow the comparison with these experimental results, the simulations have been performed in a three-dimensional model with the same dimensions of the experimental setup used for PIV measurements. The correlation between the experimental and the numerical data has been used to select the best radiation and turbulence models for the simulation of this façade typology. Main turbulent structures of the flow inside the cavity have been identified and compared. Velocity contours inside the cavity, velocity profiles as well as temperature levels have been used to evaluate the suitability of the mathematical models, and most important, to validate a simulation procedure that could be used with relative confidence, to analyse in detail the thermal behaviour of OJVF systems.

Additionally, the selected method has been applied to analyse the effect of the height of the ventilated cavity and the effects of the incident solar radiation in the convective ventilation flow. The parametrical study aims to provide some valuable information (mass flow though the joints, ventilation mass flow and pressure profiles) that could serve as benchmarking data to validate other models such as those already developed to calculate double glazed ventilated facades (DGVF): models based on energy balances (analytical [19], adimensional [20] or lumped models [21]), models based on nodal airflow networks [22], or models based in control volume discretization [23, 24].

2. Experimental set up

For this work, the experimental results have been extracted from a series of experiments performed on an open-joint ventilated façade model. The velocity vectors were measured in the vertical midsection of a laboratory OJVF model. Fig. 1 shows a sketch of the experimental set up. Experiments for three temperature conditions corresponding to Rayleigh numbers Ra= 5.92×10^8 Ra=9.19×10^8 and Ra= 1.35×10^9 were performed. A summary of the experimental work is presented in the following paragraphs. However, more details on the experimental unit, measurement procedures as well as the experiments conditions and uncertainty calculations can be found in Sanjuan et al. [18].

The PIV system used in the experiments (manufactured by the company TSI) consists of a double cavity Nd:YAG (YAG120-BSL) Laser Pulse Synchronizer, two CCD cameras (630159 Power View 4MPlus) with 4 pixel resolution and dynamic range (12 bit output). The cameras are connected to a PC equipped with a 64 bit frame grabber that acquires 16 frames per second. The Insight 3G Software has been used to control the system. The thermographs of the heated slabs have been obtained with the ThermaCam TM FLIR SC660 also from TSI.

The OJVF model is composed of four slabs made of iron and separated by horizontal open joints. The size of each tile is 30 cm wide, 20 cm high and 2 mm thick. The horizontal joints are 5 mm wide. The air cavity has a thickness of 4 cm. To produce the heating of the slabs (simulating the incident radiation), self-adhesive electrical heating mats were added to each of the four slabs. Surface temperatures were measured in the centre of each slab, and in the middle of the air channel at the height of the joints. The temperatures in the interior of the seeding box and the laboratory temperature were also recorded.

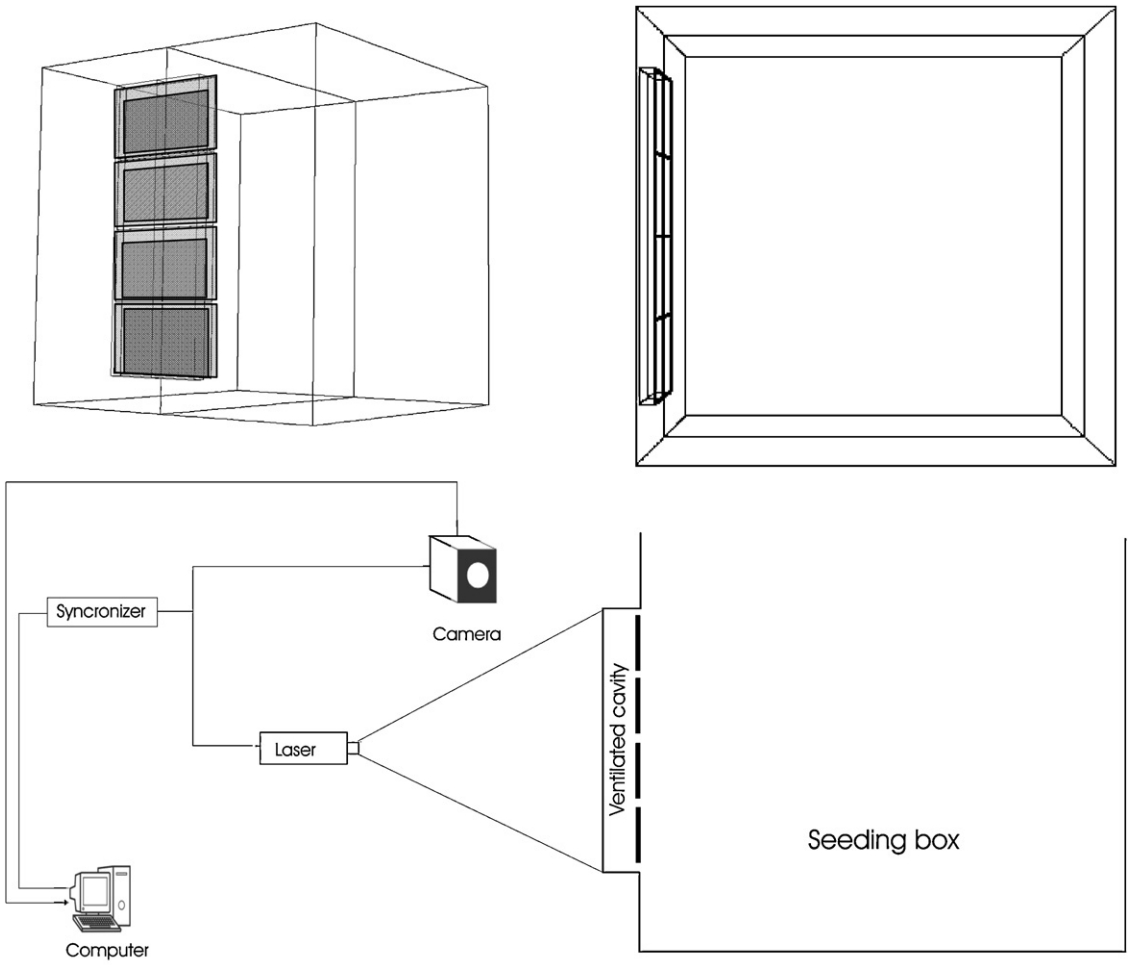

Fig. 1 Experimental set up.

Eight vertical runs were performed to analyse the whole length of the air cavity during the experiments. For each run, a total number of 300 snapshots were recorded with a frequency of 7 Hz. The processing interrogation window has been set to 40 x 40 pixels resulting in a spatial resolution of the measurement velocity field of 2.3mm x 2.3mm . The displacement vectors were computed using the standard cross correlation with a 25% overlap of the interrogation regions. Post-processing was made in order to reject the substandard vectors of each PIV realization. A further post-processing was performed to calculate the average mean velocity field for each experimental run, using the 300 instantaneous vector maps recorded at each measurement location, and to obtain the flow reconstruction along the ventilated cavity.

Following Adeyinca and Naterer [25] the total error in the measured quantities has been calculated as a sum of the bias component (B) and the precision component (P). Using the root-sum-square method for computing the total uncertainty, the relative errors for the measured peak velocity were 6.5%, 5.7% and 5.9% for experiments $Ra= 5.92x10^8$ $Ra=9.19x10^8$ and $Ra= 1.35x10^9$ respectively.

3. Numerical modelling

A general purpose computational fluid dynamic software package: Fluent [26] has been employed to perform the simulations. To allow the comparison with experimental results, the simulations have been performed in a three dimensional geometry with the same dimensions and materials as the experimental unit used for the PIV experiments: a seeding box opened on the top and the ventilated cavity on one of the lateral sides.

A mesh has been developed with a structured grid inside the ventilated cavity and a non-structured grid with tetrahedral volumes at the seeding box volume. To check the grid convergence, some tests have been performed varying the size, number (between 150.000 and 2.000.000 elements) and distribution of cells inside the ventilated façade. Tests show (see Fig. 2) that meshes with coarse cells in the near wall regions (i.e. mesh with less than 250.000 cells) fail to predict the boundary layer. A mesh size of at least 1 mm is needed in the near wall regions. The mesh tests also evidence that the centre of the cavity does not require a mesh as fine as the near wall regions. To perform the final calculations, a mesh with a total number of 500.000 cells has been used. The number of cells inside of the ventilated cavity has been optimized by refining the grid size to 1 mm in the near wall regions and progressively increasing to a maximum size of 4.5 mm in the centre regions of the cavity.

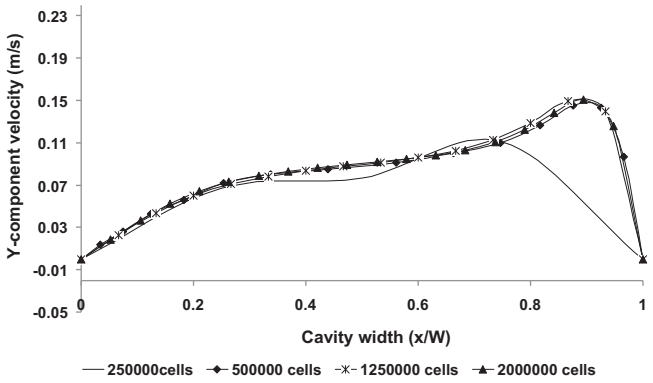

Fig. 2. Mesh tests. Cavity height y/h=0.18.

Fig. 3 shows a sketch of the boundary conditions imposed in the model. The heating of the slabs with the electrical mats has been considered in the modelling as an internal heat source in the exterior face of the slabs. The thermal boundary conditions imposed on the exterior surfaces of the box walls take into account the convective heat exchange with the laboratory indoor temperature (that was measured during the experiments). To calculate the heat transfer to the room (building interior) a convective boundary condition has been set, with a coefficient of 8 W/m^2K, corresponding to indoor air flow conditions according to the ASHRAE [27]. The top of the seeding box, which is opened in the experiments, has been modelled with constant (atmospheric) pressure and a temperature equal to the measured temperature inside the seeding box.

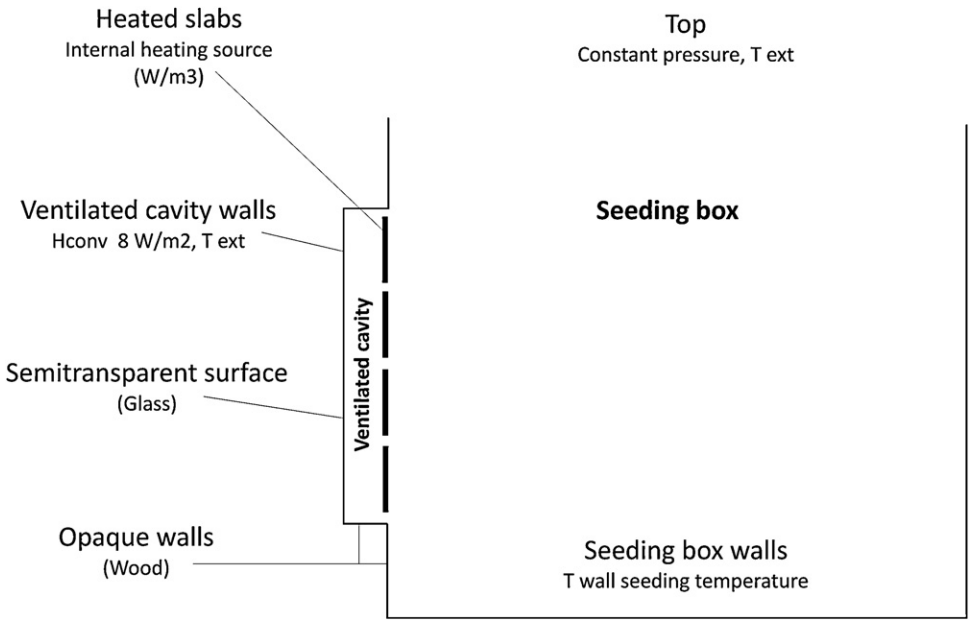

Fig.3. Boundary conditions.

The materials employed in the simulation are the same as in the experimental model. The air circulating inside the ventilated façade has been modelled as incompressible ideal gas for the density. Viscosity, heat capacity and conductivity have been included as a function of the temperature. The seeding box walls are made of wood. The slabs of the OJVF are made of iron, and the exterior walls are modelled as wood. As commented above, the PIV technique requires visual access to the flow, and two glass windows were opened in the exterior walls, these windows have been also included in the simulation model. The walls of the box are painted in black, so to model the radiation exchanges an emissivity value of 0.95 was assigned. In the glass walls, the emissivity value was set to 0.837 (UNE-EN-673 [28]).

Inside the ventilated cavity of an OJVF, and although the exterior coatings are made of opaque materials, a non negligible part of the heat transfer is produced by radiation exchange. For this reason it is very important to select the most adequate model. The simulation model is based in previous works of Sanjuan et al [13] and Gonzalez et al. [14, 15]. These works had in common that the incident radiation on the heated slabs could be introduced into the simulation domain in two different ways: a) by including the absorbed radiation as an internal source of the slabs, or b) by entering the solar radiation into the domain by using semitransparent wall boundary conditions. The second procedure has the limitation that only the Discrete Ordinate Radiation Model allows to model semitransparent walls. Still, to avoid discarding any model, several radiation models available in the CFD codes have been tested: the Rosseland model, the P1 model, the Discrete Transfer Radiation Model (DTRM) and the Discrete Ordinates model (DO).

To take into account the non-isotropic nature of the turbulence inside the ventilated cavity, due to the wall vicinity, the low Reynolds numbers, and the effects of the flow though the small joints, some further refinements have also been included in the turbulent models:

- Walls affect turbulent flows due to the high temperature and velocity gradients at the near wall regions. The mesh near the wall has been modelled fine enough to allow the enhanced wall treatment to solve the near wall region all the way to the sub laminar region. The enhanced wall treatment is a near-wall modelling method that combines a two-layer model with enhanced wall functions: a) In the two-layer approach the whole domain is subdivided into a viscosity-affected region and a fully-turbulent region. The demarcation of the two regions is determined by a wall-distance-based, turbulent Reynolds number. b) Additionally, the enhanced wall functions formulate the law-of-the-wall as a single wall law for the entire wall region by blending linear (laminar) and logarithmic (turbulent) laws-of-the-wall using a function suggested by Kader [29]. This way, the near wall regions can be solved in the laminar sub layer, buffer region, and fully-turbulent outer region.
- It is well known (Hanjali [30]), that if the turbulence Re number is small enough, viscosity affects all turbulent interactions. To this effect, the "*differential viscosity*" option has been used in the RNG k-epsilon model and in the K-omega models to activate the low-Reynolds-number modifications to turbulent viscosity.
- The turbulence generation due to buoyancy has also been included in the k-epsilon models family.

To minimize numerical errors, the set of equations were solved using a pressure-based double-precision solver, and second order upwind discretization schemes were imposed on all the transport equations. Gravitational body forces were included within the momentum equation (Coussirat et al. [5]), using the Boussinesq approximation (Gray and Giorgini [31]) to model buoyancy effects. This approximation assists the convergence of the solution when free convection is the main force driving the fluid, and helps to reduce computation time.

The mathematical models employed in the simulations are resumed in Table 1. Detailed equations and the constants values can be found in the Fluent manual [26]. To assure a good accuracy in the results, the convergence criterion of all the scaled residuals was set to 10^{-6}.

Table 1. Simulation model.

Turbulence model	Sparlat–Almaras (S–A) k-epsilon STD (KE.STD) k-epsilon RNG (KE.RNG) k-epsilon REA (KE.REA) k-omega STD (KW.STD) k-omega SST(KW.SST)
Near wall treatment	k-epsilon models: enhanced wall treatment $Y+$ [1,5] k-omega models: low Reynolds number variant $Y+$ [1,5]
Gravitational body forces	Boussinesq approximation
Radiation model	Discrete Ordinates model (DO) P1 radiation model (P1) Rosseland DTRM
Solver	Pressure-based double-precision solver Velocity gradients based in nodes Second order upwind discretization schemes
Fluid modelling	Density, viscosity, heat capacity and conductivity as a function of temperature

4. Results

In the following sections, the results of the radiation and turbulence tests are compared to the experimental data. The whole set of tests have been performed for the experimental conditions corresponding to Ra= $1.35x10^9$. The correlation between the experiments and the numerical simulation has been used to select the best fitting models. With the selected models for radiation and turbulence, the comparison between simulation and experimental results has been extended to experimental conditions corresponding to lower Rayleigh numbers Ra= $5.92x10^8$ and Ra=$9.19x10^8$. Finally, the main features of the velocity and temperature distributions are summarized.

4.1. Performance of the radiation models

Fig. 4 shows the vertical profile of the air temperature along the ventilated cavity, at the centre of the cavity (x/W=0.5). The simulation results are compared to the experimental data (EXP in the Figure) obtained in the middle section of the façade model. The x-distances have been normalized by the cavity width (W=40mm) and the y-distances have been normalized by the cavity height (H=825mm). x/W=1 correspond to the heated slabs. And y/H=1 corresponds to the top of the cavity.

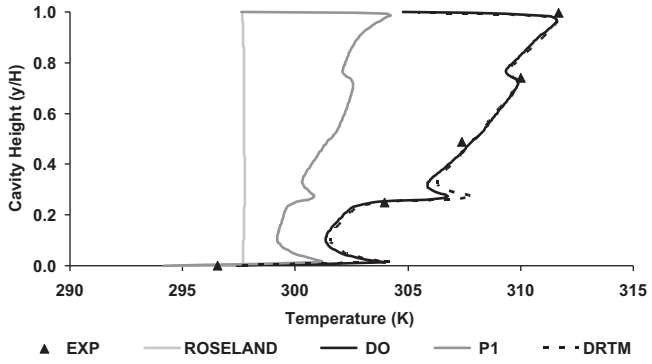

Fig. 4. Radiation tests. Air temperature inside the ventilated cavity.

The simulation results show better fit in temperature when the DO and DTRM radiation models are selected. P1 and Roseland models diverge considerably from the experimental data. Between the DO and the DTRM models, the first one has been selected to simulate OJVF because it also meets the following requisites: air as participating media in the radiative balances, take into account wall emissivities, allow to model semi-transparent walls, impose radiation boundary conditions, use of internal heating sources, and the radiation division in different length wave intervals to differentiate the long and short wave percentage of incoming radiation.

The DO model solves the radiation equations for a finite number of discrete solid angles which are defined by the code as a function of the divisions and number of pixels. For this work, the parameters have been set to 3 divisions and 16 pixels. These values are based in the work of Suarez et al. [32], which performed a parametrical study of the angular parameters for the simulation of a glazed gallery, and found that these values are a good comprise between computational resources, and accuracy of the results.

4.2. Performance of the turbulence models

To establish the capability of the different turbulence models to predict the fluid and thermal behaviour of open-joint ventilated facades, the temperature levels and velocity vector fields obtained in the different tests have been compared to PIV measurements. All the results presented in this section are referred to the middle plane of the ventilated cavity and have been performed with the DO radiation model.

Fig. 5 shows the measured and simulated vertical temperature profiles of the air along the middle of the ventilated cavity (x/W=0.5). All the different turbulence models predict fairly well the experimental results. However, the *k-epsilon* (abbreviated as KE in the Figures) family is the best fitting one. Note that the different *k-epsilon* models have very similar results, with differences smaller than 2%, and the same happens with the *k-omega* (abbreviated as KW in the Figures) models.

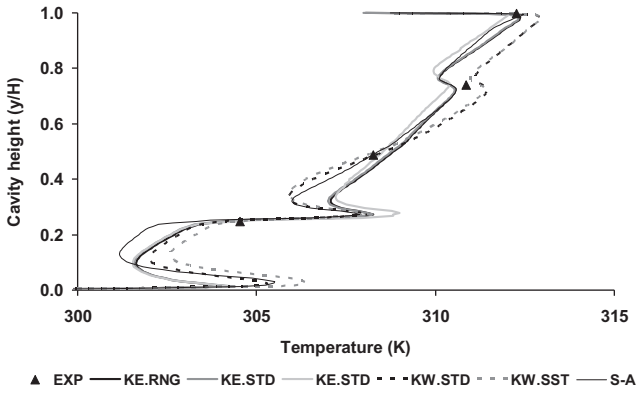

Fig.5. Turbulence tests. Air temperature inside the ventilated cavity.

Horizontal profiles for the y-velocity component at several cavity heights are represented in Fig. 6. In the Figure PIV corresponds to the experimental data and the other curves correspond to the different turbulence models that have been tested. It can be observed that the agreement between the PIV and CFD results is quite good along the cavity, with the exception of the fluid structures formed in the first slab. Best fittings occur when the *k-epsilon* models are used. As happened with the temperature profiles, the results obtained with the different *k-epsilon* models are very similar and discrepancies are smaller than 2%.

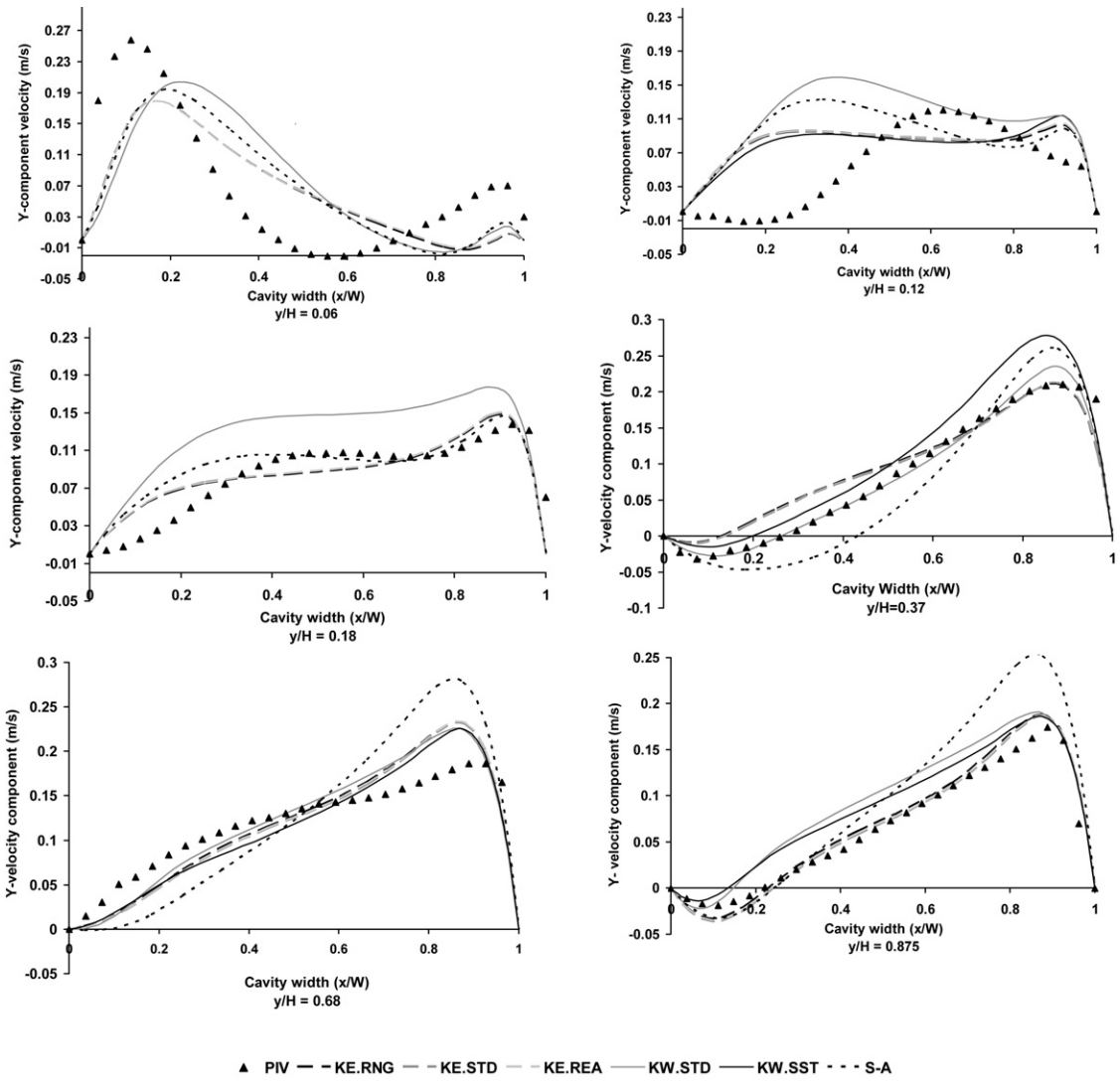

Fig.6 Turbulence tests. Y-component velocity profiles at different cavity heights.

Although experimental and numerical results show very similar trends in the flow development along the channel, localized discrepancies must be outlined. When comparing the velocity profiles at the lower slabs, two main differences can be observed: the numerical simulations under predict the size of the recirculation vortexes, and it fails to calculate the position of the flow reattachment to the heated slabs.

These discrepancies can be seen especially at the lower part of the cavity. For the height corresponding to ¼ of the first slab (y/H=0.06), the velocity profiles show that, while in the measured vectors, the main entering flow is mainly attached to the room (left) wall, in the simulations this flow is already defecting from that wall. This divergence is originated because the recirculation vortex predicted in the simulations is smaller that the measured in the experiments. These underestimations in the vortex production, produce also a discrepancy in the velocity profiles measured at the centre of the first slab (y/H=0.12). While in the experimental results the entering flow is still reattaching itself to the heated slabs, in the simulation results, an ascending flow has already developed. However, as the flow ascends in the ventilated cavity, the measured and calculated velocity shows a much better agreement, as it can be seen in the subplots corresponding to heights y/H=0.37, y/H=0.68, and y/H=0.875.

For more information, a detail of the velocity contours for the lower slabs is represented in Fig. 7. In this figure it is easy to observe how the turbulence models fail to predict the recirculation vortexes and the flow reattachment to the heated slabs. The plotted velocity field corresponds to simulation tests with the RNG *k-epsilon* turbulence model.

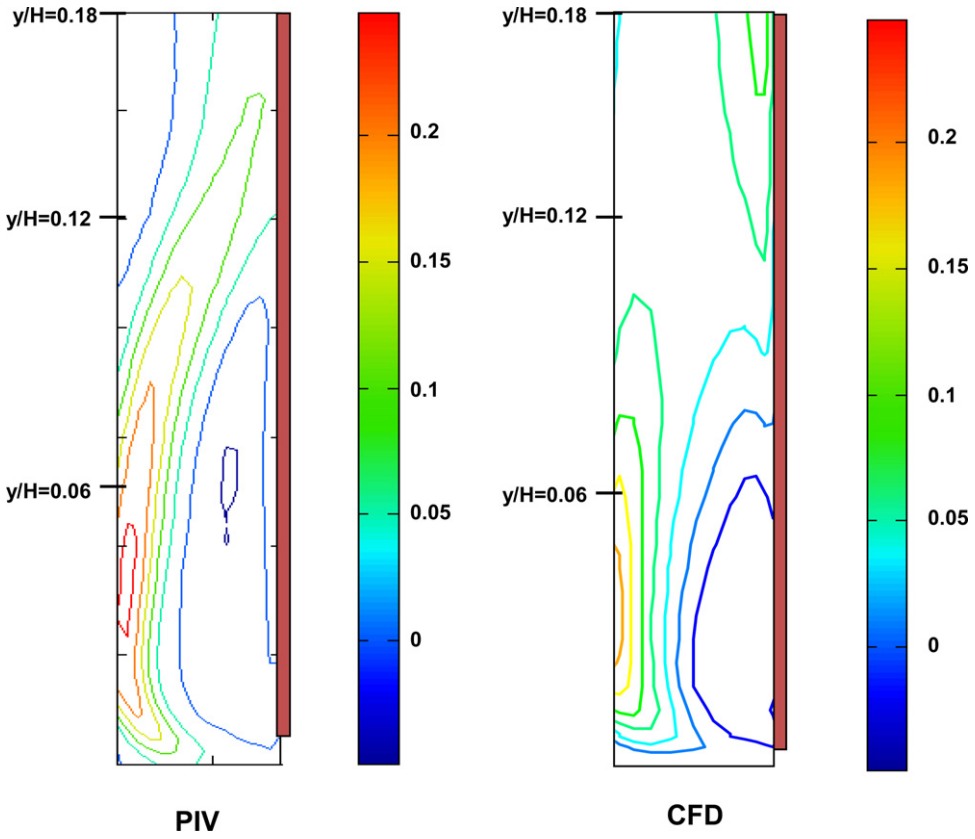

Fig 7. Detail of the velocity contours at the first slab. Measured (PIV) and simulated (CFD).

The averaged absolute errors between the measured (PIV) and simulated (CFD) velocity profiles for the three experiments corresponding to Ra= $5.92x10^8$, Ra=$9.19x10^8$ and Ra= $1.35x10^9$ are summarized in Table 2. Estimation errors of the turbulence tested models for the experiment with Ra= $1.35x10^9$ are also summarized in Table 3.

Table 2. Averaged absolute errors for the analyzed profiles.

Averaged absolute error (m/s)	$y/H = 0.12$	$y/H = 0.36$	$y/H = 65$	$y/H = 0.875$
$Ra = 5.92 \times 10^8$	0.019	0.053	0.104	0.049
$Ra = 9.19 \times 10^8$	0.022	0.023	0.023	−0.001
$Ra = 1.35 \times 10^9$	0.041	0.015	0.001	0.012

Table 3. Averaged absolute and relative errors for the analyzed profiles. Turbulence models.

Averaged absolute error (m/s)	$y/H = 0.06$	$y/H = 0.12$	$y/H = 0.18$	$y/H = 0.36$	$y/H = 65$	$y/H = 0.875$
KE.RNG	0.056	0.052	0.016	0.029	0.023	0.017
KE.STD	0.056	0.053	0.016	0.028	0.024	0.017
KE.REA	0.056	0.052	0.016	0.028	0.024	0.017
KW.STD	0.056	0.052	0.016	0.018	0.023	0.029
KW.SST	0.062	0.063	0.045	0.035	0.021	0.025
SA	0.057	0.058	0.019	0.030	0.041	0.040

4.3. Thermo fluid behaviour of OJVF

A reconstruction of the flow along the ventilated cavity is shown in Fig. 8. The numerical and experimental data show very similar trends in the flow evolution along the ventilated cavity, as it can be observed in the contour patterns.

Fig. 9 shows the temperature contours of the surface of the heated slabs. Thermograph images are compared to simulation results. The plotted contours help visualizing the cooling of the slabs produced by the flow in the cavity: Although the mean temperature of the slabs increases with the height, the temperature in the slabs is not homogeneous. The slabs are colder in the regions near the edges due to the flow through the joints.

In general terms, from the results shown here and the previous work of the authors [13, 14, 15, 16 and 18] the behaviour of the flow inside the cavity can be summarized in the following points:

- The mean flow is aligned with the cavity walls due to the effect of the buoyancy forces. The ascending ventilation flow is marked by discontinuities at the joints.
- The air enters the cavity through the joints of the lower slabs, and leaves the cavity through the joints of the upper slabs.
- Small recirculation vortexes are formed near the slabs at the entrance of the flow though the joints.
- The maximum ascending flow rate is reached at the central height of the façade.
- The same patterns are repeated for different temperature levels (Rayleigh number).
- In the absence of vertical joints (sealed or unexisting), when the open joints are only horizontal, two dimensional behaviour can be assumed in the behaviour of the OJVF.

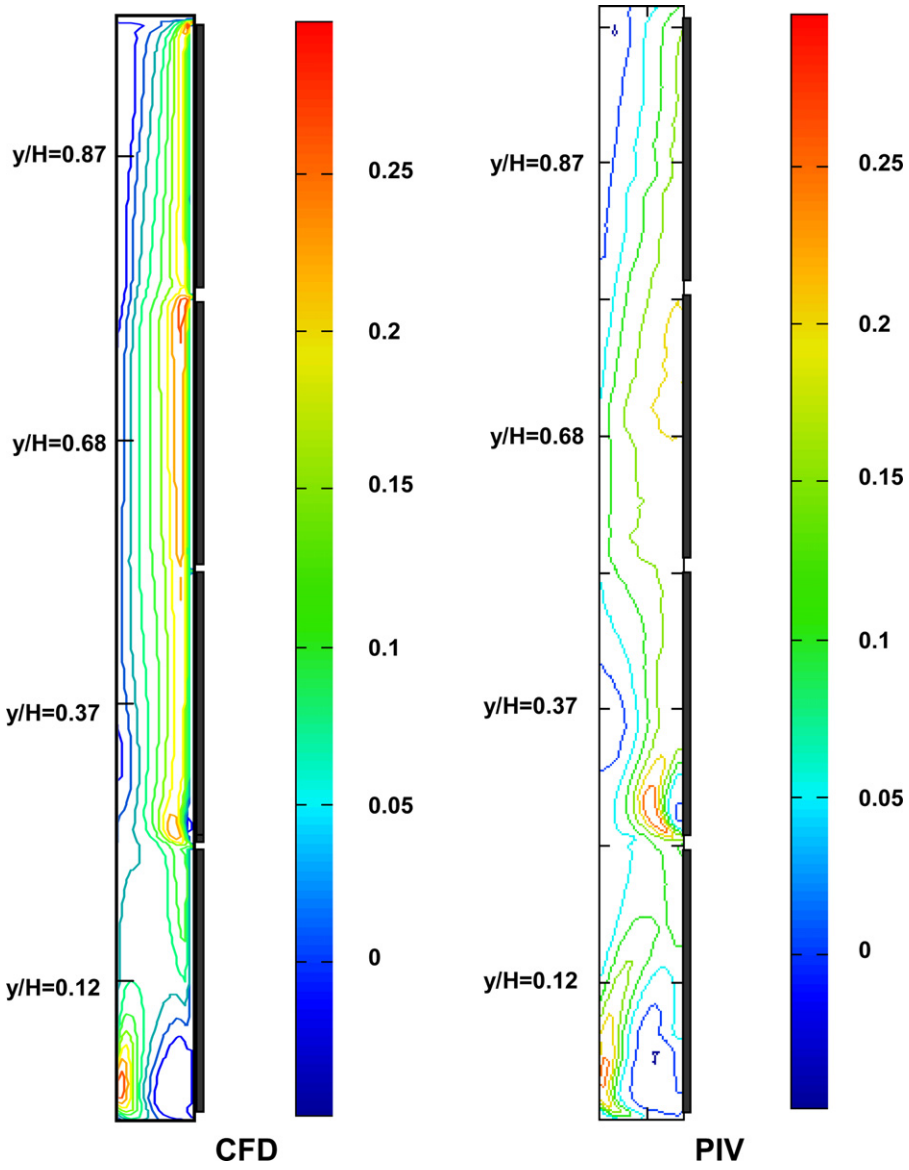

Fig 8. Velocity contours in the ventilated cavity. Measured (PIV) and simulated (CFD).

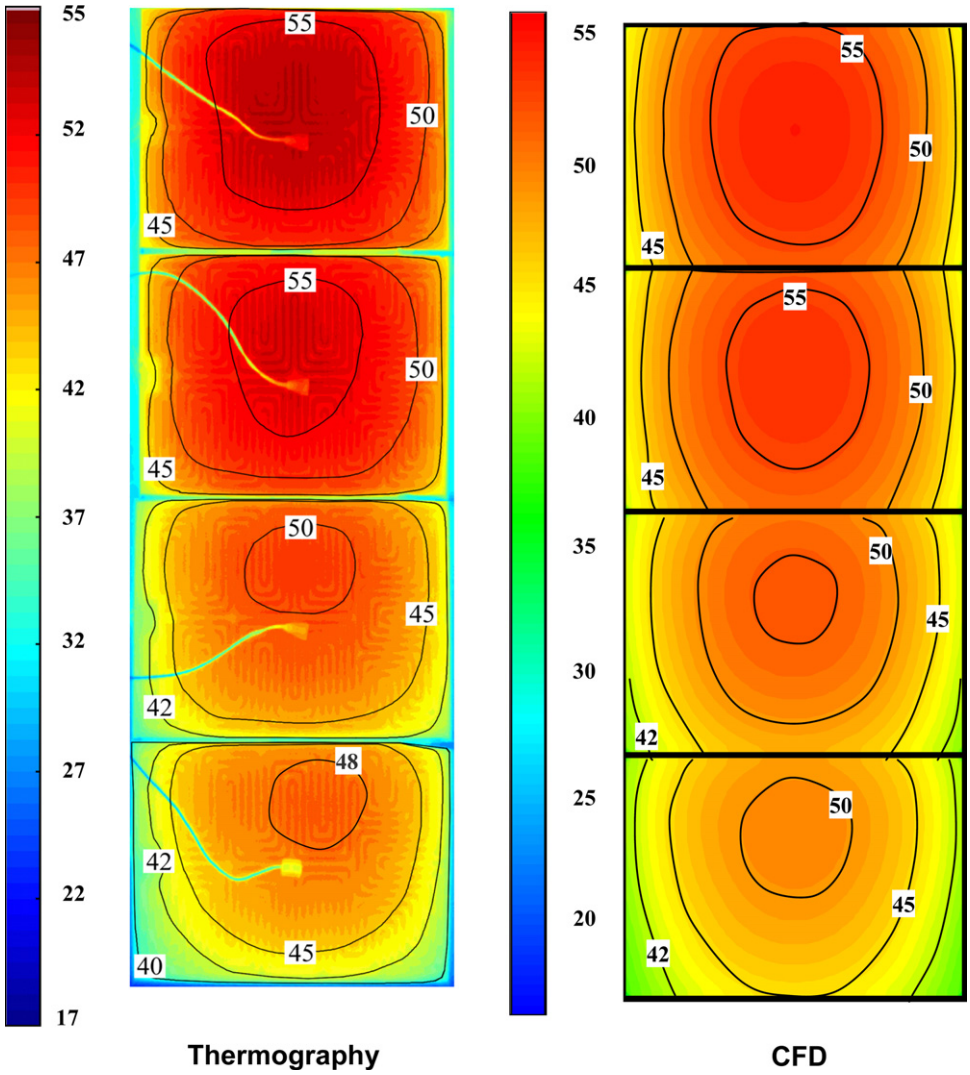

Fig 9. Temperature contours of the heated slabs. Measured (Thermograph) and simulated (CFD).

5. Ventilation flow results

One of the most claimed advantages of open joint ventilated façades is their ability to reduce cooling thermal loads. The improved thermal performance of the OJVF under radiation conditions relies on buoyancy: The slabs of the exterior coating are heated up and produce an ascending mass flow of air (by natural convection) that enters and leaves the cavity through the joints. This flow removes part of the heat loads, reducing the heat transfer to the indoor environment. This phenomenon can also be observed in other typologies of ventilated facades, with the openings located only at the bottom and top of the façade, although their efficiency is not as high in comparison to OJVF, due to the reduced flow entrance and the higher temperatures attained at the upper section of the air gap (Millar et al. [16]).

Previously cited studies have proved that the ventilation flow rate and the mass balance though the joints of the OJVF depends on the heating conditions of the slabs. With regard to the effect of the cavity height, and although none of the studies deal with the analysis of this parameter, the results coincide in the fact that regardless of the number of joints, the flow enters the cavity distributed along the slabs below the central height and leaves the cavity also distributed along the upper joints. Only at the joints located at the central height is the flow though the joints negligible (Sanjuan et al., [14]).

In order to improve the limited and dispersed knowledge about the influence of this fundamental parameter, a series of new simulations have been performed in a 2D façade model based in the above validated model. The simulated geometry is based on a commercial system that consists of:

- an external coating of ceramic slabs (slab size: 0.33 x 0.66 m and thickness 0.01 m);
- horizontal joints shaped from slab to slab, with a space of 0.005 m;
- a ventilated air gap (0.04 m width) inside of which aluminium beams for the slabs support are positioned closing the air path though the vertical joints;
- an insulation layer (thickness 0.05 m).
- a brick wall (thickness 0.12 m)

Parametrical simulations for different heights corresponding to 8, 10, 12 and 14 slabs have been performed. The outdoor air temperature has been set to 303ºC (summer conditions), the indoor ambient temperature has been set to 296ºC (comfort temperature) and the absorbed radiation has been varied from 200 to 600 W/m^2.

Fig. 10. shows the percentage of ventilation flow that enters and exits though the joints of the simulated façades for a value of absorbed radiation equal to 400 W/m^2. Negative values indicate entering flow and positive values outgoing flow.Different subplots represent the distribution of the flow for different geometries (8, 10, 12 and 14 slabs).

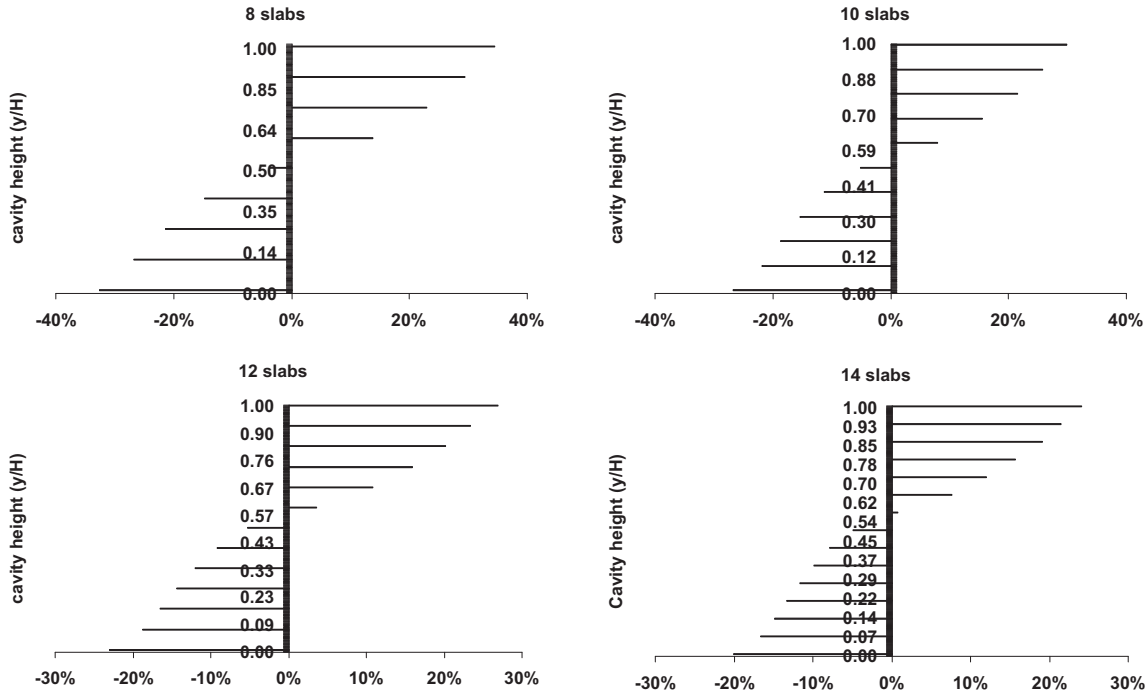

Fig. 10. Distribution of mass flow though the joints.

The subplots of Fig. 10 evidence a general pattern in the flow behaviour. The flow enters though the lower joints but not at the same rate. The total flow that enters the cavity is distributed though the joints located below the central height (y/H= 0.5), following such a pattern that the percentage of mass flow diminishes with the height of the joints. On the upper side of the cavity, the tendency is the opposite, the distribution of the exhaust mass flow increases with the height, being the higher joint the one with higher flow.

According to the represented mass flow balances, the maximum flow rate inside the ventilated cavity is achieved at the central height of the cavity. Simulation data obtained for different façade heights (number of slabs) and temperature conditions (absorbed radiation) have been represented in Fig. 11. This plot shows that the ventilation flow in OJVF is linearly enhanced by the height of the ventilated cavity and also by radiation conditions although with a non linear relation.

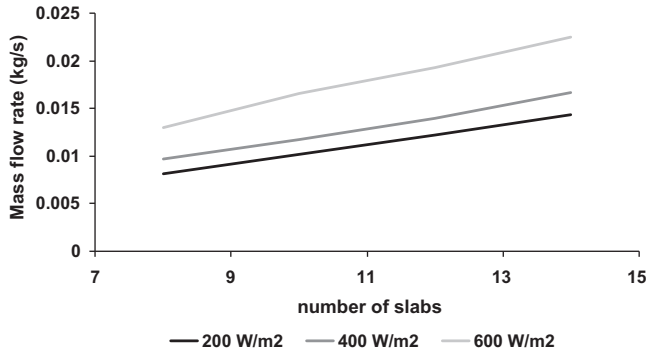

Fig.11. Ventilation mass flow rate.

The pressure levels in the cavity (x/W=0.5) have also been plotted for the geometries of 8 and 10 slabs and varying radiation (see Fig. 12). The pressure difference between the outdoor air and the cavity interior determines the mass flow rate though the joints. The pressure profiles indicate a depression in the inferior part of the cavity that forces an entering flow thought the open joints. The pressure equilibrium is achieved in the region near the central height of the façade. As the flow rises, the overpressure forces the flow to exit though the upper joints. The pressure differences inside the ventilated cavity increase with the incident radiation as well as with the height of the ventilated cavity.

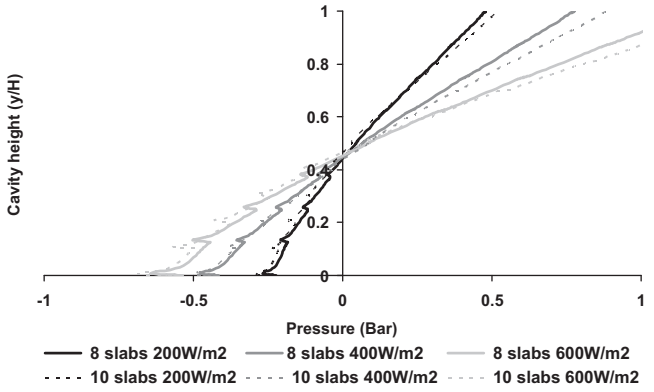

Fig.12. Pressure profiles in the ventilated cavity.

6. Conclusions

The work presented in this article aim to shed some more light on the topic OJVF. A tree-dimensional CFD model has been developed to simulate OJVF under radiation conditions and it has been validated with PIV experimental data. The suitability of the different turbulence and radiation models available in the commercial CFD codes has been investigated. Simulations have been performed on a 3D model with the same geometry, materials and boundary conditions as the experimental unit used by Sanjuan et al. [18]. The comparison between experimental and numerical data indicates that the k-epsilon two equation turbulence models and the DO radiation models show best fittings in temperature and velocity profiles. Still, all the turbulence models fail to predict the size of the recirculation vortexes formed at the entrance of the slabs.

Using the selected turbulence and radiation models, a parametrical simulation on a 2D model of a real façade have been performed. The effect of varying the cavity height (increasing the number of slabs), and different levels of incident radiation has been investigated. The results show that the ventilation produced by buoyancy (chimney effect) is enhanced by cavity height and incident radiation. Additionally, it has been found that, regardless of the number of joints, the flow enters the cavity distributed along the slabs below the central height (the percentage of entering flow diminishes with the height), and leaves the cavity also distributed along the upper joints (the percentage of the flow increases with the height). The presented 2D results (mass flow though the joints, ventilation mass flow and pressure profiles) can be used as benchmarking to validate other

models, such as those based on energy balances (analytical, non-dimensional…), lumped models, or those based on nodal airflow networks.

7. Acknowledgments

This research was done under the PSE-ARFRISOL project (reference PSE-120000-2005-1), a scientific-technical research project of singular character, supported by the National Research, Development and Innovation Plan (Plan Nacional de I+D+I) 2004-2007 from the Spanish Education and Science Authority (Ministerio de Eduación y Ciencia), funded with European Regional Development Funds (ERDF). The authors greatly thank all members of the ARFRISOL consortium for their support.

8. References

[1] H. Manz, Airflow patterns and thermal behaviour of mechanically ventilated glass double façades, Building and Environment 39 (2009) 1023–1033.

[2] N. Safer, M. Woloszyn, J.J. Roux, Three-dimensional simulation with a CFD tool of the airflow phenomena in single floor double-skin facade equipped with a venetian blind, Solar Energy 79 (2) (2005) 193–203.

[3] G. Baldinelli, Double skin facades for warm climate regions: Analysis of a solution with an integrated movable shading system, Building and Environment 44 (2009) 1107-1118.

[4] R. Fuliotto, F. Cambuli, N. Mandas, N.Bacchin, G. Manara, Q.Chen, Experimental and numerical analysis of heat transfer and airflow on an interactive building façade, Energy and Buildings 42 (2010) 23-28.

[5] M. Coussirat, A. Guardo, E. Jou, E. Egusquiza, E. Cuerva, P. Alavedra, Performance and influence of numerical sub-models on the CFD simulation of free and forced convection in double-glazed ventilated facades, Energy and Buildings 40 (2008) 1781-1789.

[6] Código Técnico de la Edificación (CTE), Ministerio de Ciencia e Innovación, Gobierno de España, 2006.

[7] Eley Associates. VisualDOE 2.5: Program Documentation, 1995.

[8] TRNSYS, A Transient System Simulation Program, Version 16. University of Wisconsin, 2004, Available from: <http://sel.me.wisc.edu/trnsys/>.

[9] EnergyPlus, Engineering Reference Manual, Building Technologies Program, U.S. Department of Energy (DOE), 2008.

[10] B. Griffith, A model for naturally ventilated cavities on the exteriors of opaque building envelopes. Proceedings of SIMBUILD2006, Cambridge-Massachusetts, USA, 2006.

[11] C. Mesado, S. Chiva, E. Juliá, L. Hernandez, Two dimensional modelling with CFD of the behaviour of a ventilated ceramic facade. In: V European Conference on Computational Fluid Dynamics ECCOMAS CFD, Lisbon, Portugal, 2010.

[12] F. Patania, A. Gagliano, F. Nocera, A. Ferlito, A. Galesi, Thermofluid-dynamic analysis of ventilated facades, Energy and Buildings, 42 (2010) 1148-1155.

[13] C. Sanjuan, M.J. Suárez, M. González, J. Pistono, E. Blanco, Energy performance of an open-joint ventilated façade compared with a conventional sealed cavity façade, Solar Energy, In Press, Corrected Proof, Available online 19 May 2011.

[14] M. González, E. Blanco, J.L. Río, J. Pistono, C. San Juan, Numerical study on thermal and fluid dynamic behaviour of an open-joint ventilated façade. In: Proceedings of PLEA 2008, Dublin, Ireland, 2008.

[15] M. González, E. Blanco, J. Pistono, Adjusting an energy simulation model by means of CFD techniques to analyze open-joint ventilated façades energy performance. In: Proceedings of WREC08, World Renewable Energy Congress X and Exhibition, Glasgow Scotland, United Kingdom, 2008.

[16] I. Millar, M.J. Suarez, E. Blanco, J. Pistono, Análisis numérico del comportamiento térmico y fluidodinámico de una fachada ventilada de junta abierta. In Spanish. In: Proceedings of I Congreso sobre Arquitectura Bioclimática y Frío Solar, Roquetas de Mar, Spain, 2010.

[17] C. Marinosci, P.A. Strachan, G. Semprini, G.L. Morini, Empirical validation and modelling of a naturally ventilated rainscreen façade, Energy and Buildings, 43 (2011) 853-863.

[18] C. Sanjuan, M.N. Sánchez, M.R. Heras, E. Blanco, Experimental analysis of natural convection in open joint ventilated Facades With 2D PIV, Building and Environment, Building and Environment, 46 (2011) 2314-2325.

[19] J. Von Grabe, A Prediction Tool for the Temperature Field of Double Facades, Energy and Buildings 34 (2002) 891-899.

[20] C. Balocco, A Non-Dimensional Analysis of a Ventilated Double Façade Energy Performance, Energy and Buildings 36 (2004) 35-40.

[21] C.S. Park, G. Augenbroe, T. Messadi, M. Thitisawat, N. Sadegh, Calibration of a Lumped Simulation Model for Double-Skin Façade Systems, Energy and Buildings 36 (2004) 1117-1130.

[22] J. Tanimoto, K. Kimura, Simulation Study on an Air Flow Window System with an Integrated Roll Screen, Energy and Buildings 26 (1997) 317-325.

[23] D. Faggembauu, M. Costa, M. Soria, A. Oliva, Numerical Analysis of the Thermal Behaviour of Ventilated Glazed Facades in Mediterranean Climates. Part I. Development and Validation of a Numerical Model, Solar Energy 75 (2003) 217-228.

[24] D. Saelens, S. Roels, H. Hens, The Inlet Temperature as a Boundary Condition for Multiple-Skin Façade Modelling, Energy and Buildings 36 (2004) 825-835.

[25] O.B. Adeyinka, G.F. Naterer, Experimental uncertainty of measured entropy production with pulsed laser PIV and planar laser induced fluorescence, International Journal of Heat and Mass Transfer 48 (2005) 1450-1461.

[26] Fluent 6.3 Documentation. Lebanon, US: Fluent Inc., 2006.

[27] ASHRAE Fundamentals handbook (S.I.), American Society of Heating, Refrigerating and Air Conditioning Engineers Inc., 1985.

[28] UNE-EN-673, Vidrio en la construcción. Determinación del coeficiente de transmisión térmica, U. Método de cálculo, 1998.

[29] B. Kader, Temperature and Concentration Profiles in Fully Turbulent Boundary Layers. International Journal of Heat and Mass Transfer, 24 (1981) 1541-1544.

[30] K. Hanjali, Advanced turbulence closure models: a view of current status and future prospects REVIEW. Int. J. Heat and Fluid Flow, 15 (3) (1994) 178-203.

[31] D.D. Gray, A. Giorgini, The validity of the Boussinesq approximation for liquids and gases. International Journal of Heat and Mass Transfer 19, (1976) 545-551.

[32] M.J. Suárez, A.J. Gutiérrez, J Pistono, E. Blanco, CFD analysis of heat collection in a glazed gallery, Energy and Buildings 43 (2011) 108-116.

Figure captions

Fig. 1 Experimental set up.

Fig. 2. Mesh tests. Cavity height y/h=0.18

Fig.3. Boundary conditions.

Fig. 4. Radiation tests. Air temperature inside the ventilated cavity.

Fig.5. Turbulence tests. Air temperature inside the ventilated cavity.

Fig.6 Turbulence tests. Y-component velocity profiles at different cavity heights

Fig 7. Detail of the velocity contours at the first slab. Measured (PIV) and simulated (CFD)

Fig 8. Velocity contours in the ventilated cavity. Measured (PIV) and simulated (CFD)

Fig 9. Temperature contours of the heated slabs. Measured (Thermograph) and simulated (CFD).

Fig. 10. Distribution of mass flow though the joints.

Fig.11. Ventilation mass flow rate.

Fig.12. Pressure profiles in the ventilated cavity.